

Article

Nonlocal and Size-Dependent Dielectric Function for Plasmonic Nanoparticles

Kai-Jian Huang ^{1,2}, Shui-Jie Qin ^{1,2,*}, Zheng-Ping Zhang ¹, Zhao Ding ¹ and Zhong-Chen Bai ²¹ College of Big Data and Information Engineering, Guizhou University, Guiyang 550025, China² Guizhou Provincial Key Lab for Photoelectron Technology and Application, Guizhou University, Guiyang 550025, China

* Correspondence: shuijie_qin@sina.com

Received: 4 July 2019; Accepted: 26 July 2019; Published: 31 July 2019



Abstract: We develop a theoretical approach to investigate the impact that nonlocal and finite-size effects have on the dielectric response of plasmonic nanostructures. Through simulations, comprehensive comparisons of the electron energy loss spectroscopy (EELS) and the optical performance are discussed for a gold spherical dimer system in terms of different dielectric models. Our study offers a paradigm of high efficiency compatible dielectric theoretical framework for accounting the metallic nanoparticles behavior combining local, nonlocal and size-dependent effects in broader energy and size ranges. The results of accurate analysis and simulation for these effects unveil the weight and the evolution of both surface and bulk plasmons vibrational mechanisms, which are important for further understanding the electrodynamics properties of structures at the nanoscale. Particularly, our method can be extended to other plasmonic nanostructures where quantum-size or strongly interacting effects are likely to play an important role.

Keywords: EELS; plasmons vibrational modes; nanoparticles; nonlocal and size-dependent dielectric

1. Introduction

Classical local electrodynamics in nanostructures under the assumption that the polarization characteristics at a given point are locally related to the external electromagnetic excitation, which has been thoroughly explored from isolated nanoparticles and dimers to other complex structures [1–5]. On the other hand, the nonlocal response of a metal nanostructure to an external disturbance stimulus determines many important plasmonic properties and has attracted much theoretical interest [6–9]. In recent years, the Mortensen group [10] have studied plasmons in metal nanoparticles by using a popular hydrodynamic model which incorporates nonlocal effects by introducing a pressure term that inhibits squashing electrons into small plasmonic nanoparticles. Similarly, the work of Christensen et al. [11] included nonlocality in the optical response of metallic nanoparticles by introducing quantum corrections obtained from first principles calculations, also using the hydrodynamic model. Ming et al. [12,13] have demonstrated a Maxwell-hydrodynamic model for studying the charge, energy and angular momentum conservation laws of high-order harmonics due to nonlocal and nonlinear interactions between electromagnetic waves and metallic metamaterials in the terahertz regime.

Meanwhile, parallel to the above remarkable progress of nonlocal properties, there has been a growing interest in exploring the quantum properties of surface plasmon and the prospects of plasma devices based on reliable operation at the quantum level. However, theoretical investigation of plasmonic resonances for nanostructure sizes ranging between 2 and 20 nm remains a challenge. This length scale is too small for classical electromagnetic theories to be valid but too large for full-fledged quantum simulations to be feasible. Therefore, some of the studies are committed

to provide a unified theoretical framework that breaks wide discrepancy between classical electromagnetic theory and quantum mechanical theory for plasmonics and nanophotonics, and ultimately control plasmonic responses in nanostructures. Crucial to this endeavor is to understand finite-size effects in nanostructures since the control of nanoparticle size represents one of the most effective approaches to harness the tremendous potentials of plasmonics and nanophotonics.

Recent studies have shown a theoretical method with a suitable modification of the bulk complex dielectric function for free and bound electrons within metallic nanoparticles [14–19], for the determination of plasma frequency, damping constants, and size distributions of noble metal nanoparticles, such as gold, silver and copper; in addition, the corresponding optical characterization deduced by Mie's theory has been tested to fit full UV-Vis experimental extinction spectra. The above theoretical framework follows the idea of Kreibig and von Fragstein [20], who considered that the augmentation of the damping constant in the Drude model results from additional collisions of free electrons with the particle boundary, as well as the idea of Inouye et al. [21], who took into account the interband transitions of bound electrons for the complex dielectric function. Consequently, the metal dielectric function can be regarded as the sum of the free (intraband transitions) and bound (interband transitions) electron contributions; then, a size-dependent (SD) dielectric function (Equation (4)) based on a stepwise modification of the Drude model is put forward. Under this theoretical framework, the significant finite-size effects of optical properties for metallic nanoparticles can be expected to be observed below a certain limited size range (e.g., valid restriction of 20 nm drawn from Refs. [14,15]).

A developed microscopic approach based on accurate inclusion of the Lorentz friction for the plasmon damping within the random phase approximation (RPA) model [22–24] has also been performed in recent years. Unlike the conventional Mie's theory that only gives reasonably intrinsic size effects for nanospheres of radii lower than 5 nm in vacuum due to neglecting the Lorentz friction losses that dominate over all attenuation channels, the specific size dependence for plasmons due to the Lorentz friction induced corrections derived upon this theoretical approach can be applied to account for the observed irregular size-effect of plasmon resonance for relatively large metallic nanoparticles (e.g., for Au nanospheres of radii 20–60 nm in vacuum drawn from Ref. [24]). This theoretical approach has also been verified to improve experimental data fitting of metallic nanospheres measured in water colloidal solutions, especially pronounced for a large size limit (e.g., of radii 10–75 nm for Au nanospheres in water colloidal solutions drawn from Ref. [22]). One should note that, although accurate accounting for the Lorentz friction is important for nanospheres of radii above 20 nm (for Au in vacuum), the major drawback of our work is that adequate corrections of the Lorentz friction are not included, since integrating them with the nonlocal and size-dependent effects within a macroscopic material dielectric function is not straightforward.

Extending beyond the nonlocal and size-dependent effects we have focused on, in the following, there is a huge amount of research concerning about other “non-classical electromagnetic effects” by incorporating some “quantum effects” within classical electrodynamics. Quantum-size effects due to the confinement of electron motion in small dimensions can lead to a discrete electronic energy levels and a size-dependent conductivity [25]. Accessing plasmonic modes in the quantum tunneling regime also remains as a challenge, quantum tunneling effects become significant for subnanometer interparticle gaps and can be reflected through a quantum corrected model (QCM), which models the junction between adjacent nanoparticles by means of a local dielectric response that includes electron tunneling and tunneling resistivity at gap [26,27]. However, such “non-classical” effects are of great interest and significance in the field of nano-optics, and can be incorporated into classical electrodynamic descriptions for some simple systems; directly integrating them within a general framework is not straightforward. In particular, quantum tunneling effects between metal nanoparticles will not be considered in this work.

Nonlocal effects are a direct consequence of the inhomogeneity of the electron gas, and can hardly be ignored when the mean free path of an electron in the simple systems is larger than the wavelength of light [28,29]. To a certain extent, nonlocal electrodynamics partially account for finite-size and

quantum mechanical effects inherent in a nanostructure in a more rigorous way. Such as in the case of applying the hydrodynamic dielectric function to calculate the absorption coefficient from metallic nanoparticles, its size-dependent effects will show up by an effective dielectric function due to the additional boundary conditions for solving polarizabilities [30]. Although it has been argued that the hydrodynamic model yields only semiquantitative results in the linear regime, recent improvements regarding the incorporation of interband transitions and Landau damping have demonstrated that fully quantitative results may be obtained [31,32]. In principle, as most of the modified hydrodynamic models shown in the aforementioned applications, a spatially nonlocal relationship between the material polarization and the field of plasmonics can typically be mirrored through the use of a spatially nonlocal dielectric function. Some of them take finite-size effects of the nanostructure into consideration by using a modified collision frequency. However, the corresponding changes in optical, plasmonic and dielectric responses are almost negligible, and the effective dimension of nanostructure for nonlocal electrostatics is also being limited or obscured consequently.

Inspired by the studies of the size-dependent dielectric function as mentioned above, in this paper, we move a step forward in this direction by developing nonlocal and size-dependent (NLSD) dielectric approach that incorporates the spatially local, nonlocal, size and even analogous quantum-size responses of the material. As an example, we investigate how the electron energy loss spectroscopy (EELS) and optical responses of gold spherical dimers of various radii and inter-particle gaps are modified once the nonlocality and finite-size effects are considered. These examples allow for a straightforward interpretation of our results. Unlike those complex configurational and resource consuming methods, such as quantum mechanical simulations based on the time-dependent Kohn–Sham density functional theory (TD-KSDFT), our approach provides a powerful and simple tool to calculate and analyze the EELS and optical response ranging from classical to quantum regimes.

2. Methods and Theoretical Framework

Figure 1 displays the fundamental system under study; a dimer consists of two closely spaced freestanding metallic nanospheres of radius R , and a certain distance d apart. The system is excited by an electron beam with high kinetic energy up to 200 keV passing by or penetrating through at the positions as indicated in the figure, and illuminated from the top by a plane wave polarized along the dimer axis, respectively. For this study, the metal is assumed to be gold, and the experimental and theoretical values of permittivity for contrast taken from Johnson and Christy [33] and Werner et al. [34], respectively. We chose the data models above for comparison for the following reasons. First, of all, in general, *ab initio* density functional theory (DFT) approaches need to deal with pseudopotentials, and include quantum effects that completely change the spectral distribution and the field enhancements of the plasmon resonant modes supported by a given nanostructure; they are computationally demanding and are currently limited to small-sized nanoparticles with a few thousand electrons (e.g., valid restriction of 12.3 nm drawn from Ref. [35]). Second, the application of classic local experimental dielectric data for small-sized nanoparticles ranging between 2 and 20 nm becomes questionable as described in the Introduction. These factors will be discussed in detail below combined with calculation results. All of the numerical simulations are implemented via the general public license toolbox MNPBEM [36,37], which is based on a boundary element method (BEM) approach.

The dielectric function of noble metal nanoparticles (e.g., Cu, Au, and Ag) is well described by using the hydrodynamical Drude model limit by three components [38–40]:

$$\varepsilon_{\text{Nonlocal}}(\mathbf{k}, \omega) = \varepsilon_{\infty} + \varepsilon_{\text{inter}}(\omega) + \varepsilon_{\text{intra}}(\mathbf{k}, \omega), \quad (1)$$

where the \mathbf{k} dependence in $\varepsilon_{\text{Nonlocal}}(\mathbf{k}, \omega)$ is necessary to describe the spatially nonlocal response of structures with features less than 10 nm [41,42]. ε_{∞} is the value as $\omega \rightarrow \infty$. $\varepsilon_{\text{inter}}(\omega)$ represents

the contribution from interband electron transitions and can be physically described in the form of a Lorentz oscillator model,

$$\epsilon_{\text{inter}}(\omega) = \sum_j \frac{\Delta\epsilon_{Lj}\omega_{Lj}^2}{\omega_{Lj}^2 - \omega(\omega + i2\delta_{Lj})}. \quad (2)$$

In this work, we take index $j = 2$ labeling the individual d-band to sp-band electron transitions since there are two interband transitions in Au at optical frequencies [33]. $\epsilon_{\text{intra}}(\mathbf{k},\omega)$ is responsible for the intraband effects which are usually referred to as free-electron effects, where both the plasmonic optical response of metals and nonlocal effects are contained and can be described by

$$\epsilon_{\text{intra}}(\mathbf{k},\omega) = -\frac{\omega_D^2}{\omega(\omega + i\gamma) - \beta^2\mathbf{k}^2}, \quad (3)$$

where ω_D is the plasma frequency, γ is the collision frequency, and β is the hydrodynamical parameter measuring the degree of nonlocality. For the three-dimensional situation $\beta^2 = 3v_F/5$, where $v_F = 1.39 \times 10^6$ m/s is the Fermi velocity for the Au nanoparticles. Then, all parameters in Equations (2) and (3) can be estimated by fitting Equation (1) to the experimentally determined dielectric data of bulk Au in Ref. [33]. Here, we use all the parameters taken from Ref. [39], $\omega_D = 8.812$ eV, $\gamma = 0.0752$ eV, $\epsilon_\infty = 3.559$, $\Delta\epsilon_{L1} = 2.912$, $\omega_{Lj} = 4.693$ eV, $\delta_{L1} = 1.541$ eV, $\Delta\epsilon_{L2} = 1.272$, $\omega_{Lj} = 3.112$ eV, $\delta_{L1} = 0.525$ eV.

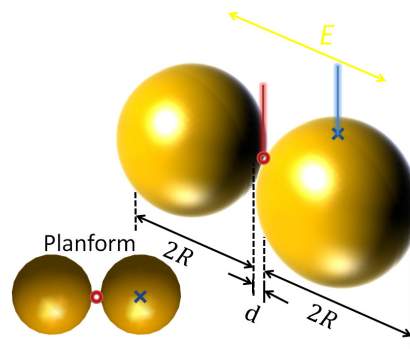


Figure 1. Schematic illustration of the system under study: the interaction of the electron beam passes by or penetrates through a dimer consisted with two Au nanospheres with radius R and gap d, as well as the plane wave polarized along the dimer axis. The inset shows the exact located positions (or impact parameters) of electron beams: the red ring represents the middle of the gap and the blue cross represents the centre in one of the nanospheres.

Note that the above dielectric function calculation model neglects quantum-mechanical exchange and correlation effects, but the significant nonlocal effects from the reduced mean free path of the conduction electrons due to electron–interface scattering in small metal structures can be taken into account by using a modified collision frequency $\gamma' = \gamma + 4Av_FV/S$ in Equation (3) for the three-dimensional problems [43]. In principle, conclusions from the previous studies that adopt such modified collision frequency have shown that the Nonlocal model of Equation (1) can model the spatially nonlocal dielectric response of arbitrarily shaped and sized structures [39,40]. However, although the volume of the structure V and surface area S in the modified collision frequency implies the influence of size factor, only the impact of free electrons was considered to be modified by size. In addition, correctly selecting the value of dimensionless parameter A remains a challenging since its complex details are of discrepancy in different theoretical dielectric models (consult Section 1 in Ref. [44] and its references for a detailed discussion). Therefore, in order to overcome this difficulty in a classical mean free path approach, a more reasonable alternative way for describing size-dependent dielectric functions is needed by considering the dominated conditions and a scope of the contributions of intraband transitions (free electrons) and interband transitions (bound electrons). Herein, according to

previous studies about suitable modification of the bulk complex dielectric function for free and bound electrons within metallic nanoparticles [14–16], the full size-corrected dielectric function can be written as the sum of three terms:

$$\varepsilon_{SD}(\omega, R) = \varepsilon_{\text{bulk}}(\omega) + \Delta\varepsilon_{\text{free}}(\omega, R) + \Delta\varepsilon_{\text{bound}}(\omega, R), \quad (4)$$

where $\varepsilon_{\text{bulk}}(\omega)$ corresponding to the experimentally measured bulk values from UV-visible to NIR-FIR, and the last two terms are size-corrective contributions for free and bound electrons, respectively:

$$\Delta\varepsilon_{\text{free}}(\omega, R) = -\omega_D^2 \sum_{n=1}^{\infty} (-1)^n \frac{(i\omega C v_F / R)^n}{(\omega^2 + i\omega\gamma_{\text{free}})^{n+1}}, \quad (5)$$

$$\Delta\varepsilon_{\text{bound}}(\omega, R) = -K_b e^{R/R_0} \int_{\omega_g}^{\infty} \frac{\sqrt{x - \omega_g}}{x} [1 - F(x, T)] \frac{dx}{x^2 - \omega^2 + \gamma_{\text{bound}} - 2i\omega\gamma_{\text{bound}}}, \quad (6)$$

where $\hbar\omega_g$ is the gap energy; $F(x, T)$ is the Fermi distribution function of conduction electron of energy $\hbar x$ and temperature T with Fermi energy E_F , $\gamma_{\text{free}} = \gamma$, γ_{bound} stands for the damping constant in the band to band transition; K_b is a proportionality factor with units of $s^{-3/2}$; C is a constant that depends on the material. For noble metals, it has a value of about 0.8 that has been theoretically justified from first principles calculations [45]; R_0 is a reference radius value that represents the range for which the density of states can be considered to reach the value of the bulk. For Au, the following values determined in Refs. [14–16] were used: $\omega_g = 2.1062$ eV, $\gamma_{\text{bound}} = 0.158$ eV, $K_b = 2.3 \times 10^{24} s^{-3/2}$, $E_F = 2.5$ eV.

Note that the interband transitions from the d-band to the conduction sp-band near the L point in the Brillouin zone can be taken into account by the size-corrective contribution for bound electrons in the form of Equation (6) [46]. Because of the nonlocal dielectric function, $\varepsilon_{\text{Nonlocal}}(\mathbf{k}, \omega)$ is estimated by fitting Equation (1) to the complex bulk dielectric function, which is the local, frequency-dependent part of the response, taken from optical measurements given in Ref. [33] and exactly the same as the first term $\varepsilon_{\text{bulk}}(\omega)$ using the size-dependent dielectric function $\varepsilon_{SD}(\omega, R)$ of Equation (4); we adopt here the former as a substitute for the latter. The resulting nonlocal and size-dependent (NLS) dielectric function of the metal is thus approximated by

$$\varepsilon_{\text{NLS}}(\mathbf{k}, \omega, R) = \varepsilon_{\text{Nonlocal}}(\mathbf{k}, \omega) + \Delta\varepsilon_{\text{free}}(\omega, R) + \Delta\varepsilon_{\text{bound}}(\omega, R). \quad (7)$$

3. Results and Discussion

The first example of the compatible effectiveness produced by our NLS approach is shown in Figure 2 for comparisons of EELS calculated with different dielectric models and gold spherical dimers of different sizes, where electron beam penetrates the centre in one of the nanospheres (Figure 2a) and passes by the middle of the gap (Figure 2b) as shown in Figure 1, and the gap d fixed on 1 nm. Figure 2a shows that the agreement of the total energy loss probabilities between the NLS approach (black solid line) and the theoretical dielectric data set (green dashed line), which is obtained from density functional theory (DFT) calculations by Werner et al. [34], is remarkable for radii up to 20 nm. Moreover, for the NLS approach, the evolves of the size-dependent response as the radius increases are observably more outstanding than the full size-dependent dielectric model (blue dotted line, Equation (4)), and the total energy loss probabilities become almost consistent with those calculated by using the local, frequency-dependent and experimental complex bulk dielectric values (red dash-dotted line) as radii up to 100 nm.

In addition, blueshifts of the main energy loss peaks become more apparent as the radius increases and it is accompanied by plasmon broadening. These nonlocal effects are known as the availability of

the additional loss channels [7], and can have an effect in the higher energy region when compared to classical local electrodynamics because of the interplay between ω and \mathbf{k} in Equation (3). All of the above agreements between the model predictions support that our approach provides a straightforward theoretical framework to describe metal behavior combining local, nonlocal and size-dependent effects in broader energy and size ranges simultaneously.

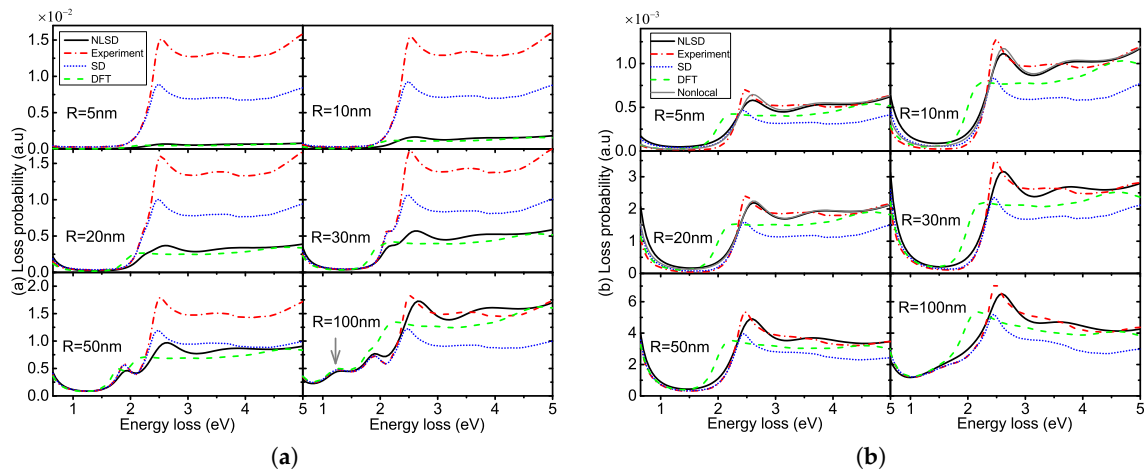


Figure 2. EELS (electron energy loss spectroscopy) spectrums for Au spherical dimers of different radii R , and for different dielectric models (black solid curves, NLSD (nonlocal and size-dependent) model; blue dotted curves, SD model; red dash-dotted curves, experimental dielectric data from Johnson et al. [33]; green dashed curves, DFT (density functional theory) calculated data from Werner et al. [34]; thinner gray solid curves, Nonlocal model), where the gap d fixed on 1 nm. (a) electron beam penetrating the centre in one of the nanospheres, and (b) passing by the middle of the gap, respectively, as indicated in Figure 1.

Moreover, according to the various developed theories of the SD model as mentioned in Section 1, the significant finite-size effects on the optical properties of nanoparticles can only be expected to be observed below a certain limited size range of about 20 nm. Our model captures the main aspects of the finite-size effects for small-sized nanoparticles. For radii below 20 nm, Figure 2b shows a significant difference of the total (and surface) energy loss probabilities between the NLSD approach and nonlocal dielectric model (thinner gray solid curves) of Equation (1). $A = 0.1$ was used in the modified collision frequency $\gamma' = \gamma + 4Av_F V/S$ when using the Nonlocal model [39,40]. In addition, unlike the outcomes between the SD model and the experimental dielectric data, which show remarkable differences in all size range, the total (and surface) energy loss probabilities calculated by using the NLSD model are almost identical with the Nonlocal model for radii larger than 20 nm this is why the forecasted results of Nonlocal model are not shown in Figure 2b where the radii larger than 20 nm. Similarly, for clarity, Figure 2a does not show the outcomes from the Nonlocal model because they are identical with those from the NLSD model in all size ranges.

In consideration of the size-corrective terms from SD and NLSD model being the same, these results might appear unexpected at the first view. The nonlocal effects themselves are also size-dependent. This can be seen from Figure 2b where radii are below 20 nm; besides capturing the blueshifts, the main energy loss peaks of the Nonlocal model are obviously less than those by using experimental dielectric data, but in a low-energy region (e.g., 0.65–2.4 eV), the outcomes of the Nonlocal model are higher than those by using experimental dielectric data, which have the same changing tendency as the results of SD and NLSD models. However, the NLSD model is a more suitable implementation for revealing the contribution of the surface vibrational mode with nanoparticles of the small radius. When compared with the Nonlocal model, the outcomes of the NLSD show that the relative reductions in the main energy loss peaks, and the increases of the outcomes in the low-energy

region are more remarkable, as shown in Figure 2b. All of these are because the size-dependent effects due to the size-corrective terms are contained in the NLSD model.

For further confirmation of the present findings, EELS calculated with different dielectric models for isolated Au spherical nanoparticles of different sizes are presented in Figure 3, where electron beam passing near the nanoparticles and the contribution of the surface vibrational mode is dominant. The difference of the total (and surface) energy loss probabilities between the NLSD model and Nonlocal model becomes more pronounced with the reduction of particle size, as shown in Figure 3 where the radius $R = 1$ nm, and the prediction of our NLSD model are much more close to the outcomes from the SD model and the DFT model. The discrepancy in predicted energy loss probabilities between the NLSD model and the Nonlocal model would gradually narrow and ultimately disappear when the radius is greater than 26 nm, as shown in Figure 3b, in addition to the discrepancy in predicted energy loss probabilities between the SD model and experimental dielectric data. These results for isolated nanoparticles are more compatible with the conclusions that have been verified both experimentally and theoretically in the previous studies of the SD model in which the significant size-dependent effects can only be expected to be observed below a certain limited size range of approximately 20 nm.

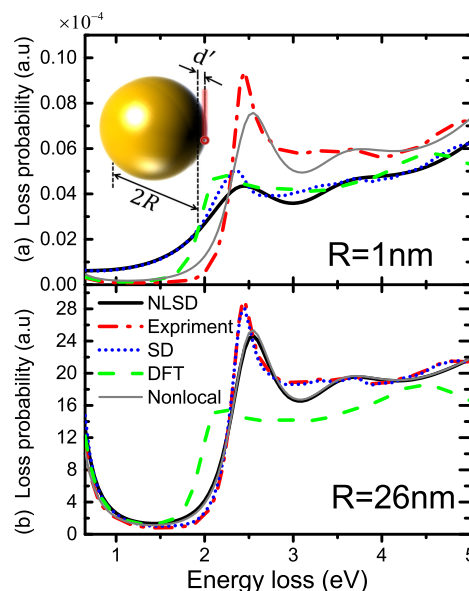


Figure 3. EELS spectrums for isolated Au spherical nanoparticles of different radii R , and for different dielectric models as defined in the text, when electron beam passing near the nanoparticles as depicted in the inset. Distances d' between electron beam and nanoparticles were fixed at 2 nm.

Although, under what specific physical mechanism will the differences due to the size-dependent effects between the SD model and experimental dielectric data disappear in the outcomes between the NLSD and Nonlocal model for dimers of a large radius merit further investigation. However, according to all of the above results of EELS, one can see that the NLSD model presented in this paper has the advantage of clearly separating the size regions where local, nonlocal or size-dependent effects are dominant, for both simulation cases (isolated particle or dimer).

First, the size-dependent effects somehow can be revealed in small isolated nanoparticles by using the SD model, whereas the outcomes of this model do not contain any appreciable impact of the nonlocal effects. In addition, at least, for dimers of a large radius, the outcomes of the SD model should be much more consistent with those by using the classic local experimental dielectric data—particularly for an electron beam penetrating the centre in one of the nanospheres and the contribution of the bulk vibrational mode being dominant, as shown in Figure 2a. By contrast, the size-dependent effects due to the same size-corrective terms in the NLSD model have been

demonstrated that, while they can be completely neglected for Au dimers of all size when the contribution of the bulk vibrational mode is dominant (Figure 2a), and, for Au dimers of a large radius, when the contribution of the surface vibrational mode is dominant (Figure 2b), they still have a great influence on dimers of a small radius, just as the results have been demonstrated for isolated particles (Figure 3).

Second, we should notice that the classic local experimental dielectric data used in this paper was obtained from reflection and transmission measurements on vacuum-evaporated thin films at room temperature [33]; the application of such local continuum electrodynamics for small-sized nanoparticles becomes questionable. This can be attributed to two effects. First of all, their imaginary part of the interband contribution due to size-dependent effects is not negligible in the spectral region of surface plasmon polariton resonance [14,15]. Second, nonlocal effects due to the scattering of the conduction electrons arise as the nanoparticle size is decreased, relative to metal films [39,40]. By contrast, either the EELS results or the optical properties that are going to be demonstrated in the following have shown that outcomes from our NLSD model can fit the DFT model better than other models for small-sized nanoparticles. These agreements benefit from the first term in the NLSD model, namely, the Nonlocal model of Equation (1), which have the advantage of describing the dynamical optical response of structures that are too large to treat using quantum mechanics but too small for classical electromagnetic theories to be valid [39,40].

It should be noted that a consistent energy loss with peak near 1.25 eV when the radius $R = 100$ nm (as indicated by the inset gray arrow in Figures 2a and 4(upper)), which is similar to the main plasmon resonances, will be presented below in Figure 6a for the extinction cross sections excited by optical plane wave, from approximately 955 nm. In order to gain physical insight into the origin of these common resonances in both situations of excitations, the surface and bulk configurations that form the total loss probabilities where $R = 100$ nm are plotted in Figure 4, respectively. The results shown in Figure 4 indicate that the total loss probabilities near 1.25 eV for any dielectric model are all dominated by surface loss probabilities. In addition, it is interesting that we found that the total energy loss probabilities shown in Figure 2b are also dominated by the surface loss probabilities, since all the bulk loss probabilities are almost zero when the electron beam located in the middle of the gap (not shown). We attribute this surface energy loss dominating effect to the contribution of the surface vibrational mode.

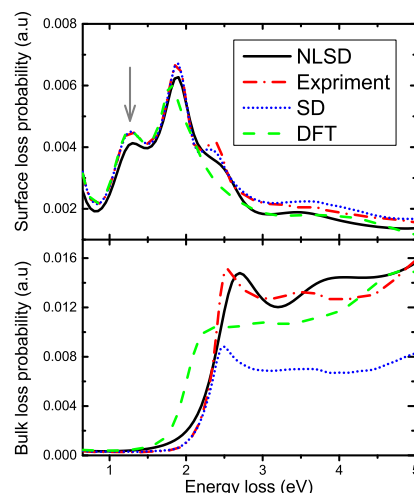


Figure 4. (Upper panel) Surface and (lower panel) bulk loss probabilities for gold spherical dimers of radius $R = 100$ nm, where the other simulation configurations remain the same as defined in Figure 2a.

One should note that, at least for now, the main energy loss peaks as depicted in Figure 2a are the coupling contribution of the surface and the bulk vibrational modes. However, it can be seen that these surface energy loss peaks near 1.25 eV as shown in Figure 4(upper) do not show up in

Figure 2b where the contribution of the surface vibrational mode is dominant. In addition, according to our surface loss probability calculation results (not shown, similar to the form of Figure 4(upper)), they also do not show up when $R = 50$ nm where the other simulation configurations remain the same as defined in Figure 2a. However, the reducing contribution of the surface vibrational mode with nanoparticles of the small radius can be distinctly revealed by the NLSM model. For example, Figure 5 plots the simulated EELS probability maps of our dimer system with four different dielectric models for the 1.25 eV resonances. Our model captures the main aspects of the nonlocal electrostatics for small-sized nanoparticles.

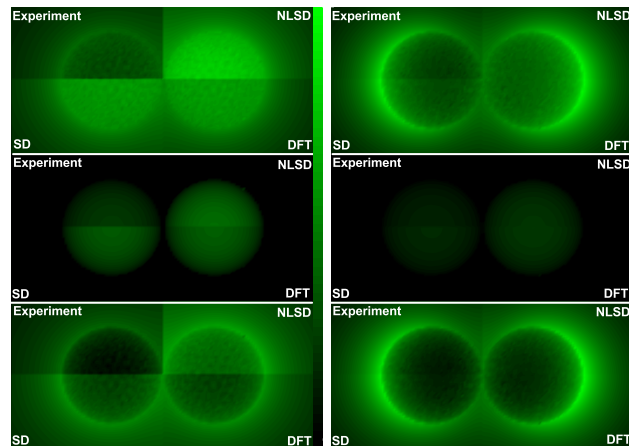


Figure 5. Total (top panels), bulk (middle panels) and surface (bottom panels) EELS probability maps for the gold dimers with particles radii $R = 20$ nm (left column) and $R = 50$ nm (right column), and for different dielectric models as defined in the text. The inter-particle gap $d = 1$ nm.

For radius $R = 20$ nm, the surface and bulk vibrational modes by using the NLSM model are higher than the others as shown in the middle and bottom panel of Figure 5 (left column). Thus, the energy loss extended throughout the whole surface of the gold spherical dimer, whereas those by using experimental dielectric data are confined in narrow rings formed by the surface and the horizontal cross-section of the dimer, as the total EELS probabilities shown in the left-top panel in Figure 5. We found similar results for dimers with radii less than 20 nm, except that the intensities of the energy loss calculated by using the NLSM approach the DFT model as the radius decreases.

For radius $R = 50$ nm, the total energy loss confined more strongly in narrow rings formed by the surface and the horizontal cross-section of the dimer for all dielectric models, and they are dominated by surface vibrational mode, as indicated by the EELS probability maps shown in Figure 5 (right column). We also found similar results for dimers with radii greater than 50 nm, except that the patterns of the total (and surface) energy loss changing from the narrow rings to crescents as the radius increases. These results mean that the nonlocal impact on the mode evolution of EELS and responses from the quantum mechanical mechanism can also be depicted by using our NLSM model. Although there are similar outcomes of mode evolution by using the SD and DFT models, they are obviously incompatible with the classic local experimental data where the size of the dimer becomes larger, such as shown in Figure 2 (e.g., $R = 100$ nm).

Finally, we use our NLSM approach to explore another interesting compatible effectiveness for the optical properties of the dimer system illuminated by a plane wave as defined in Figure 1. Although the effects of quantum natural and nonlocality have different origins, their impact on the optical response of the nanostructure can be measured by its physical parameters (in our case, which means the radius and gap). Figure 6a renders the maximum plasmonic resonances of extinction cross-sections that correspond to different radius for gold spherical dimers with the constant gap $d = 1$ nm, and for different dielectric models. The comparison between predictions from our NLSM model and the

other dielectric models clarifies how nonlocality and quantum mechanical effects modify the optical properties of the system.

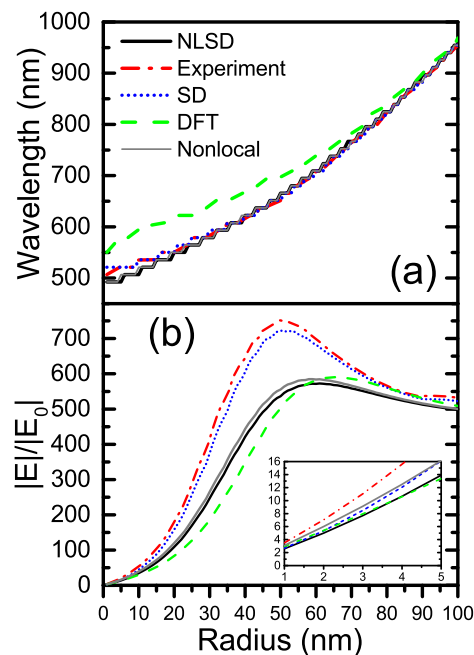


Figure 6. (a) maximum plasmonic resonances of extinction cross-sections that correspond to different radius for gold spherical dimers with constant inter-particle gap $d = 1$ nm, and for different dielectric models as defined in text; (b) maximum field enhancement at the middle point of the inter-particle gap (the red circle depicted in Figure 1) as a function of R for gold spherical dimers and their corresponding plasmonic resonances as shown in (a).

For small radii (approximately less than 35 nm), there are significant blueshifts for the prediction of our NLSD model when compared to the predictions of SD model and experimental dielectric data, which are similar to the comparison results by using another entirely different nonlocal dielectric model of the metal from previous studies (see Figure 2 or Figure 4a in Ref. [7]), and can be accounted for the inclusion of nonlocal effects in the NLSD model, which also means that the size-dependent effects due to the size-corrective terms in the NLSD model can not affect the maximum plasmonic resonances of extinction cross-sections, since the predictions of our NLSD model and the SD model are approximately consistent with those of the Nonlocal model and experimental dielectric data, respectively, as shown in Figure 6a. One should note that these maximum plasmonic resonances of extinction cross-sections that correspond to different radius for gold spherical dimers of radii ranging between 20 and 60 nm may be more accurate if our model can be integrated with the adequate corrections of the Lorentz friction. However, nevertheless, either our NLSD model or the RPA approach included with the Lorentz friction induced corrections as discussed in Section 1 has observed anomalous shift of plasmonic resonance for nanoparticles with radii significantly exceeding the previously suggested limiting 5 nm by Mie's theory.

Figure 6b renders the field enhancement $\frac{|E|}{|E_0|}$ at the middle point of the gap as a function of R for gold spherical dimers and their corresponding plasmonic resonances as shown in Figure 6a. Quite different from the extinction spectral profiles predicted, Figure 6b shows approximate tendency between the NLSD model and the DFT model. This means that the impacts of nonlocality and quantum confinement can be compatible, and both reduce the enhancement of fields. The quantum confinement effects are important when the mean free path of valence electrons is comparable to the particle size, and the mean free path of electrons in gold at room temperature is below 50 nm. These play a large role in interpreting the discrepancy in predicted field enhancements between the NLSD model and

experimental dielectric data would gradually narrow when the radius is greater than 50 nm, as shown in Figure 6b. Similar behavior occurs for the prediction of the DFT model, except that the radius which stands out for such change is approximately 65 nm. We attribute this difference to the inclusion of nonlocal and finite-size effects in the NLSM model, which lead to an increase in the contribution of the bulk vibrational mode and to reduce the contribution of the surface vibrational mode when the radius becomes less than 50 nm and gradually decreases, as the EELS results (Figure 5) discussed above. Both effects are not exclusive of small particles as the inset shown in Figure 6b.

In addition, they are also important for small inter-particle gaps since the strongly interacting between metallic geometries encountered in plasmonics. For example, as one can see from the maximum field enhancement as a function of separation for gold dimer with $R = 50$ nm shown in Figure 7, the predictions of the NLSM model and the DFT model are closely similar, and the gaps in predicted field enhancements between them and the SD model and the experimental dielectric data would gradually narrow or even vanish as the inter-particle gap d increases. As we can see both in Figures 6b and 7, between NLSM and nonlocal models, there is also a slight difference in their outcomes with a radius of less than approximately 65 nm (Figure 6b), or with a gap of less than approximately 0.5 nm (Figure 7). These are entirely caused by the size-dependent effects due to the size-corrective terms of the NLSM model, which also lead to a decreasing trend in the outcomes of the NLSM model toward the DFT model, particularly for dimers with small radii as the inset shown in Figure 6b. Furthermore, we also should note that the maximum field enhancement shown in Figure 7 may be not very accurate when the inter-particle gap d decreases below 0.5 nm, since the NLSM model may not be capable of calculating the quantum tunneling effects under such subnanometer gaps, as mentioned in Section 1.

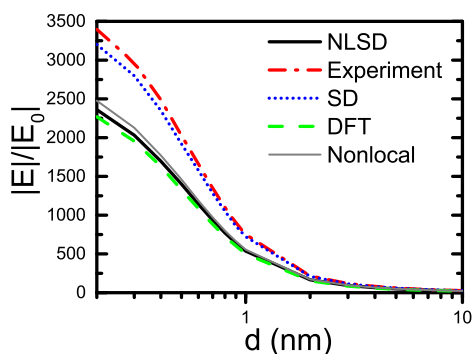


Figure 7. Maximum field enhancement as a function of separation for gold dimer with $R = 50$ nm, and for different dielectric models as defined in text (and depicted in Figure 2).

4. Conclusions

In conclusion, we presented a simplified theoretical model to describe the nonlocal and size effects of nanoparticles. Our implementation is based on the hydrodynamic Drude model and two size-corrective terms derived from the size-dependent dielectric function. We have demonstrated the compatible effectiveness and the accuracy of our theoretical model through comparisons to analytical results of the EELS and the optical responses for gold spherical dimers. These analytical results demonstrated a number of effects that result from nonlocality and finite-size effects in the dielectric response, including analogous quantum confinement effects that decrease the electromagnetic field enhancement and their corresponding weight relations of the contributions of surface and bulk vibrational modes reflected by EELS, blueshifts of surface plasmon resonances and main energy loss peaks. From these results, we can state that the nonlocal effects are of great significance as they obviously determine the blueshifts of surface plasmon resonances for the gold dimers with radii smaller than approximately 35 nm and the electromagnetic field enhancement for the gold dimers with radii ranging from 20 to 50 nm. In addition, blending the adequate size-dependent effects and nonlocal effects can more accurately reflect reductions in the main energy loss peaks and the electromagnetic

field enhancement due to quantum confinement effects for the gold dimers with radii smaller than approximately 20 nm, as well as the weight relations of the contributions of surface and bulk vibrational modes for the gold dimers with radii ranging from 1 to 50 nm; for the gold dimers with radii larger than 50 nm, the nonlocal effects in the EELS and optical responses decrease as the radii increase further, and the local effects almost dominate the EELS and optical responses as radii up to 100 nm.

Our NLSM model used here accounts for the plasmonic nanoparticles behavior combining local, nonlocal and size-dependent effects, and reconciles the discrepancy between classical electromagnetic theory and quantum mechanical theory for plasmonics and nanophotonics in broader energy and size ranges. Importantly, although we have focused on gold spherical dimers, our approach can be extended to motivate new, and more precise experimental studies on other metallic nanostructures with complex configurations, particularly those where quantum-size effects and strongly interacting effects are likely to play a large role. In the future, we expect that our approach will make possible a deep exploration of the dissipative quantum electromagnetics, where couple loss or dissipation in a quantum system to a bath of oscillators maintained a strong connection with the classical electromagnetic system [47].

Author Contributions: Conceptualization, K.-J.H.; Formal analysis, K.-J.H.; Funding acquisition, Z.-C.B.; Methodology, K.-J.H.; Supervision, S.-J.Q.; Writing—original draft, K.-J.H.; Writing—review and editing, S.-J.Q., Z.-P.Z., Z.D. and Z.-C.B.

Funding: This research was funded by the National Natural Science Foundation of China (Grant No. 61741505) and the Guizhou Province Science and Technology Projects (No. QKHZ [2017]2887).

Conflicts of Interest: The authors declare no conflict of interest.

References

1. Encai, H.; Schatz, G.C. Electromagnetic fields around silver nanoparticles and Dimers. *J. Chem. Phys.* **2004**, *120*, 357–366.
2. Amir, R.S.; Suhaidi, S.; Yap, W.F. Nanoplasmonic Sensor Based on Surface Plasmon-Coupled Emission: Review. *Appl. Sci.* **2019**, *9*, 1497.
3. Jacak, J.; Jacak, W. Plasmons and Plasmon–Polaritons in Finite Ionic Systems: Toward Soft-Plasmonics of Confined Electrolyte Structures. *Appl. Sci.* **2019**, *9*, 1159. [[CrossRef](#)]
4. Huigao, D.; Fernández-Domínguez, A.I.; Michel, B.; Maier, S.A.; Yang, J.K.W. Nanoplasmonics: Classical down to the nanometer scale. *Nano Lett.* **2012**, *12*, 1683–1689.
5. Xu, H. Theoretical study of coated spherical metallic nanoparticles for single-molecule surface-enhanced spectroscopy. *Appl. Phys. Lett.* **2004**, *85*, 5980–5982. [[CrossRef](#)]
6. David, C.; Abajo, F.J.G.D. Spatial Nonlocality in the Optical Response of Metal Nanoparticles. *J. Phys. Chem. C* **2011**, *115*, 19470–19475. [[CrossRef](#)]
7. Abajo, F.J.G.D. Non-local effects in the plasmons of strongly interacting nanoparticles, dimers, and waveguides. *J. Phys. Chem. C* **2008**, *112*, 17983–17987. [[CrossRef](#)]
8. Esquivel-Sirvent, R.; Schatz, G.C. Spatial Nonlocality in the Calculation of Hamaker Coefficients. *J. Phys. Chem. C* **2012**, *116*, 420–424. [[CrossRef](#)]
9. Moeferd, M.; Kiel, T.; Sproll, T.; Intravaia, F.; Busch, K. Plasmonic modes in nanowire dimers: A study based on the hydrodynamic Drude model including nonlocal and nonlinear effects. *Phys. Rev. B* **2018**, *97*, 075431. [[CrossRef](#)]
10. Raza, S.; Bozhevolnyi, S.I.; Wubs, M.; Mortensen, N.A. Nonlocal optical response in metallic nanostructures. *J. Phys. Condens. Matter* **2015**, *27*, 183204. [[CrossRef](#)]
11. Christensen, T.; Yan, W.; Jauho, A.P.; Soljačić, M.; Mortensen, N.A. Quantum corrections in nanoplasmonics: Shape, scale, and material. *Phys. Rev. Lett* **2017**, *118*, 157402. [[CrossRef](#)] [[PubMed](#)]
12. Fang, M.; Huang, Z.X.; Sha, W.E.I.; Xiong, X.Y.; Wu, X. Full hydrodynamic model of nonlinear electromagnetic response in metallic metamaterials. *Prog. Electromagn. Res.* **2016**, *157*, 63–78. [[CrossRef](#)]
13. Fang, M.; Shen, N.H.; Sha, W.E.I.; Huang, Z.X.; Koschny, T.; Soukoulis, C.M. Nonlinearity in the Dark: Broadband Terahertz Generation with Extremely High Efficiency. *Phys. Rev. Lett.* **2019**, *122*, 027401. [[CrossRef](#)] [[PubMed](#)]

14. Herrera, L.J.M.; Arboleda, D.M.; Schinca, D.C.; Scaffardi, L.B. Determination of plasma frequency, damping constant, and size distribution from the complex dielectric function of noble metal nanoparticles. *J. Appl. Phys.* **2014**, *116*, 233105. [[CrossRef](#)]
15. Herrera, L.J.M.; Arboleda, D.M.; Santillán, J.M.J.; Raap, M.B.F.V.; Scaffardi, L.B.; Schinca, D.C. Nanoscale Dielectric Function of Fe, Pt, Ti, Ta, Al, and V: Application to Characterization of Al Nanoparticles Synthesized by Fs Laser Ablation. *Plasmonics* **2016**, *12*, 1813–1824. [[CrossRef](#)]
16. Scaffardi, L.B.; Tocho, J.O. Size dependence of refractive index of gold nanoparticles. *Nanotechnology* **2006**, *17*, 1309–1315. [[CrossRef](#)]
17. Schinca, D.C.; Scaffardi, L.B.; Videla, F.A.; Torchia, G.A.; Moreno, P.; Roso, L. Silver-silver oxide core-shell nanoparticles by femtosecond laser ablation: Core and shell sizing by extinction spectroscopy. *J. Phys. D Appl. Phys.* **2009**, *42*, 215102–215109. [[CrossRef](#)]
18. Santillán, J.M.J.; Videla, F.A.; Schinca, D.C.; Scaffardi, L.B.; Raap, M.B.F.V. Analysis of the structure, configuration, and sizing of Cu and Cu oxide nanoparticles generated by fs laser ablation of solid target in liquids. *J. Appl. Phys.* **2013**, *113*, 134305–134309. [[CrossRef](#)]
19. Santillán, J.M.J.; Videla, F.A.; Raap, M.B.F.V.; Muraca, D.; Scaffardi, L.B.; Schinca, D.C. Influence of size-corrected bound-electron contribution on nanometric silver dielectric function. Sizing through optical extinction spectroscopy. *J. Phys. D Appl. Phys.* **2013**, *46*, 435301. [[CrossRef](#)]
20. Kreibig, U.; Fragstein, C.V. The Limitation of Electron Mean Free Path in Small Silver Particles. *Z. Für Phys. A Hadron. Nucl.* **1969**, *224*, 1307–1323. [[CrossRef](#)]
21. Inouye, H.; Tanaka, K.; Tanahashi, I.; Hirao, K. Ultrafast dynamics of nonequilibrium electrons in a gold nanoparticle system. *Phys. Rev. B* **1998**, *57*, 11334–11340. [[CrossRef](#)]
22. Jacak, W. Lorentz Friction for Surface Plasmons in Metallic Nanospheres. *J. Phys. Chem. C* **2015**, *119*, 6749–6759. [[CrossRef](#)]
23. Jacak, W. Size-dependence of the Lorentz friction for surface plasmons in metallic nanospheres. *Opt. Express* **2015**, *23*, 4472–4481. [[CrossRef](#)] [[PubMed](#)]
24. Kluczyk, K.; Jacak, W. Damping-induced size effect in surface plasmon resonance in metallic nano-particles: Comparison of RPA microscopic model with numerical finite element simulation (COMSOL) and Mie approach. *J. Quant. Spectrosc. Radiat. Transf.* **2016**, *168*, 78–88. [[CrossRef](#)]
25. Trivedi, N.; Ashcroft, N.W. Quantum size effects in transport properties of metallic films. *Phys. Rev. B Condens. Matter* **1988**, *38*, 12298. [[CrossRef](#)] [[PubMed](#)]
26. Ruben, E.; Andrei, G.B.; Peter, N.; Javier, A. Bridging quantum and classical plasmonics with a quantum-corrected model. *Nat. Commun.* **2012**, *3*, 825.
27. ShuFen, T.; Lin, W.; Joel, K.W.Y.; Ping, B.; Michel, B.; Christian, A.N. Quantum plasmon resonances controlled by molecular tunnel junctions. *Nat. Commun.* **2014**, *343*, 1496–1499.
28. Jones, W.E.; Kliewer, K.L.; Fuchs, R. Nonlocal Theory of the Optical Properties of Thin Metallic Films. *Phys. Rev.* **1969**, *178*, 1201–1203. [[CrossRef](#)]
29. Chang, R.; Leung, P.T. Nonlocal effects on optical and molecular interactions with metallic nanoshells. *Phys. Rev. B* **2006**, *73*, 125438. [[CrossRef](#)]
30. Fuchs, R.; Claro, F. Multipolar response of small metallic spheres: Nonlocal theory. *Phys. Rev. B Condens. Matter* **1987**, *35*, 3722–3727. [[CrossRef](#)]
31. Mortensen, N.A.; Raza, S.; Wubs, M.; Sondergaard, T.; Bozhevolnyi, S.I. A generalized non-local optical response theory for plasmonic nanostructures. *Nat. Commun.* **2014**, *5*, 3809. [[CrossRef](#)] [[PubMed](#)]
32. Toscano, G.; Straubel, J.; Kwiatkowski, A.; Rockstuhl, C.; Evers, F.; Xu, H.; Mortensen, N.A.; Wubs, M. Resonance shifts and spill-out effects in self-consistent hydrodynamic nanoplasmonics. *Nat. Commun.* **2015**, *6*, 7132. [[CrossRef](#)]
33. Johnson, P.B.; Christy, R.W. Optical Constants of the Noble Metals. *Phys. Rev. B* **1972**, *6*, 4370–4379. [[CrossRef](#)]
34. Werner, W.S.M.; Glantschnig, K.; Ambrosch-Draxl, C. Optical Constants and Inelastic Electron-Scattering Data for 17 Elemental Metals. *J. Phys. Chem. Ref. Data* **2009**, *38*, 1013. [[CrossRef](#)]
35. Xiang, H.P.; Zhang, X.; Neuhauser, D.; Lu, G. Size-Dependent Plasmonic Resonances from Large-Scale Quantum Simulations. *J. Phys. Chem. Lett.* **2014**, *5*, 1163–1169. [[CrossRef](#)] [[PubMed](#)]
36. Hohenester, U.; Trügler, A. MNPBEM—A Matlab toolbox for the simulation of plasmonic nanoparticles. *Comput. Phys. Commun.* **2012**, *183*, 370–381. [[CrossRef](#)]

37. Ratnanather, J.T.; Kim, J.H.; Zhang, S.; Davis, A.M.J.; Lucas, S.K. Algorithm 935: IIPBF, a MATLAB toolbox for infinite integral of products of two Bessel functions. *Acm Trans. Math. Softw.* **2014**, *40*, 131–162. [[CrossRef](#)]
38. Boardman, A.D. *Electromagnetic Surface Modes*; Wiley: New York, NY, USA, 1982.
39. McMahon, J.M.; Gray, S.K.; Schatz, G.C. Calculating Nonlocal Optical Properties of Structures with Arbitrary Shape. *Phys. Rev. B* **2010**, *82*, 035423. [[CrossRef](#)]
40. McMahon, J.M.; Gray, S.K.; Schatz, G.C. Optical properties of nanowire dimers with a spatially nonlocal dielectric function. *Nano Lett.* **2010**, *10*, 3473–3481. [[CrossRef](#)]
41. Agarwal, G.S.; Pattanayak, D.N.; Wolf, E. Electromagnetic-Fields In Spatially Dispersive Media. *Phys. Rev. B* **1974**, *10*, 1447–1475. [[CrossRef](#)]
42. Anderegg, M.; Feuerbacher, B.; Fitton, B. Optically Excited Longitudinal Plasmons in Potassium. *Phys. Rev. Lett.* **1971**, *27*, 1565–1568. [[CrossRef](#)]
43. Coronado, E.A.; Schatz, G.C. Surface plasmon broadening for arbitrary shape nanoparticles: A geometrical probability approach. *J. Chem. Phys.* **2003**, *119*, 3926–3934. [[CrossRef](#)]
44. Pinchuk, A.; Kreibitz, U.; Hilger, A. Optical properties of metallic nanoparticles: Influence of interface effects and interband transitions. *Surf. Sci.* **2004**, *557*, 269–280. [[CrossRef](#)]
45. Alvarez, M.M.; Khoury, J.I.; Schaaff, T.G.; Shafiqullin, M.N.; Vezmar, I.; Whetten, R.L. Optical Absorption Spectra of nanocrystal gold molecules. *J. Phys. Chem. B* **1997**, *101*, 3706–3712. [[CrossRef](#)]
46. Rosei, R.; Antonangeli, F.; Grassano, U.M. d bands position and width in gold from very low temperature thermomodulation measurements. *Surf. Sci.* **1973**, *37*, 689–699. [[CrossRef](#)]
47. Sha, W.E.I.; Liu, A.Y.; Weng, C.C. Dissipative Quantum Electromagnetics. *IEEE J. Multiscale Multiphy. Comput. Tech.* **2018**, *3*, 198–213. [[CrossRef](#)]



© 2019 by the authors. Licensee MDPI, Basel, Switzerland. This article is an open access article distributed under the terms and conditions of the Creative Commons Attribution (CC BY) license (<http://creativecommons.org/licenses/by/4.0/>).